WEP Warwick Evans Publishing

International Journal of Mechanical and Electrical Engineering

ISSN: 3005-9615 (Print), ISSN: 3005-7132 (Online) | Volume 3, Number 3, Year 2024
DOI: https://doi.org/10.62051/ijmee.v3n3.03
Journal homepage: https://wepub.org/index.php/IJMEE/index

Time-varying Meshing Stiffness Calculation of Spur Gears with Asymmetric Spalling Defects

Wenqiang Han *, Hanjun Jiang

College of Mechanical and Automotive Engineering, Qingdao University of Technology, Qingdao, China

* Corresponding Author: Wenqiang Han

ABSTRACT

Gear systems are subjected to repeated loads during long-term operation, and factors such as insufficient lubricant to increase friction between gears, resulting in elevated temperatures and wear, are highly susceptible to tooth spalling. Tooth spalling is a common form of failure in gear failure. In previous studies, the vibration response of a gear pair with spalling defects at the tooth center near the pitch circle has been investigated. However, the location of the spalling defects offset from the center of the tooth flank is rarely studied. Tooth spalling faults occur in the pitch circle, but not necessarily in the center of the tooth, often formed on both sides of the center of the tooth and torsion in the meshing process. the symmetric and asymmetric rectangular spalling defects are considered, the torsional deformation is introduced. “torsional stiffness” is introduced into the overall TVMS due to the spalling defect. Therefore, it is meaningful to grasp the reasons for the formation of tooth spalling.

KEYWORDS

Tooth Spalling; Asymmetric Rectangular Spalling; Torsional Stiffness.

1. INTRODUCTION

Gears are important transmission components and are widely used in industries such as airplanes, high speed railways, and automobiles [1-2]. Among them, stiffness excitation is one of the main sources of excitation for gear meshing, and calculating accurate gear tooth meshing stiffness [3-6] is an important task in gear dynamics. Gear defects that occur due to cyclic load excitation on the teeth or overloading of the gear, fatigue of the gear teeth, and insufficient lubrication are tooth spalling [7-8].

Gear time-varying meshing stiffness is one of the important parameters affecting the dynamic characteristics of the gear drive system, which has an impact on the vibration and stability of the gear system, based on the potential energy method [9-11] and finite element method [12-13] for the calculation of TVMS. The fault-containing gear system is more important to take appropriate measures for diagnosis to avoid problems [14].

Spalling is one of the common gear tooth defects, which affects the smoothness of gear tooth meshing, and has been studied by many scholars [15-22].Yang et al. [15] modeled the early stage of flaking faults as flaking faults, and investigated the gear system dynamics.Chaari et al. [16] considered the effect of flaking and other faults on the bending stiffness, the gear substrate stiffness, and contact stiffness, and calculated and analyzed the TVMS for the faulty gear system. The time-varying meshing stiffness for spalling and other faults was calculated and analyzed.Shao et al [17] carried out

an in-depth study on the gear tooth edge contact phenomenon caused by spalling faults in order to improve the accuracy of the calculation of TVMS for spalling faults.Ma et al [18,19] analyzed the effect of spalling in the time-varying meshing stiffness.Jiang et al [20] considered the meshing in helical gears containing spalling defects to The time-varying contact stiffness is obtained by changing the position and time-varying sliding friction is considered.Han et al [21] investigated the effect of flaking and localized damage on the time-varying meshing strength of helical gears by using the integral method and potential energy method. The size and location of the defects are important parameters to be considered in the calculation of their time-varying meshing stiffness.Saxena et al [22] firstly proposed the torsional stiffness in the wheel tooth stiffness in a gear model with axial misalignment resulting in misalignment of the mesh.Saxena et al [23] analyzed the effect of different flake shapes, flake sizes and locations on the mesh stiffness, and proposed the torsional stiffness induced by flake failure. Wang et al [24] analyzed the double impact response induced by spalling defects, considered asymmetric spalling defects, and also introduced the torsional deformation.The torsional stiffness calculations of Saxena and Wang, both of which directly assumed the distance between the load acting point of the torsional moment equivalent and the midpoint of the tooth meshing line as the torsional force arm, were too contingent. In addition, both of them neglected the change of the rest of the tooth stiffness components except the torsional stiffness in the region affected by spalling defects.

In view of the above problems, this paper proposes a slicing method to consider the center-symmetric spalling on the non-tooth surface, which slices the gear model on the tooth surface, obtains the related torsional force arm according to the spalling location and size, and uses the energy method to obtain the torsional stiffness and time-varying meshing stiffness of the gear teeth.

2. IMPROVED TVMS MODELING OF TOOTH SPALLING

2.1. Conventional Spalling Time-varying Meshing Stiffness Models

The traditional model mostly uses a rectangular groove to simulate the shape of spalling [19], which is symmetric around the middle of the tooth face and occurs mostly at the pitch circle of the gear tooth. As shown in the figure1, the flaking start position (flaking distance from the base circle of the gear), flaking width, flaking length and flaking depth are recorded as: L, r, w_i, h_i. When the wheel tooth contact occurs in the flaking range, the meshing gear teeth due to the reduction of the contact area leads to increased tooth deformation at this time, the wheel tooth cross-section changes.

Based on the energy method, the compression deformation energy, bending deformation energy and shear deformation energy of the gear pair with symmetric spalling defects are calculated as follows:

$$U_{ai} = \frac{F^2}{2k_{ai}}, U_{bi} = \frac{F^2}{2k_{bi}}, U_{si} = \frac{F^2}{2k_{si}} \tag{1}$$

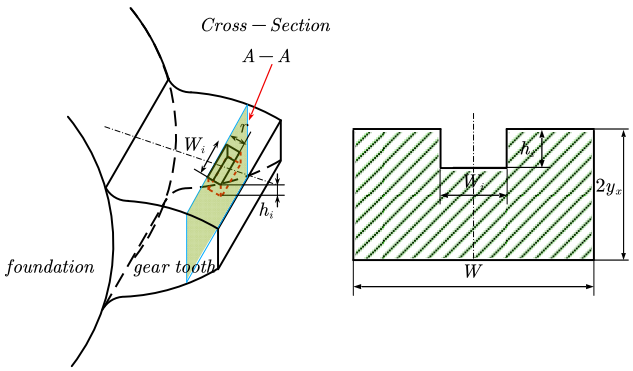

Figure 1. Sketch maps of a spall tooth

Where i=p,g, represent the pinion and large gear respectively. f is the force at the meshing of the gear teeth, ka,kb,ks are the compression stiffness, bending stiffness and shear stiffness of the gear teeth respectively.

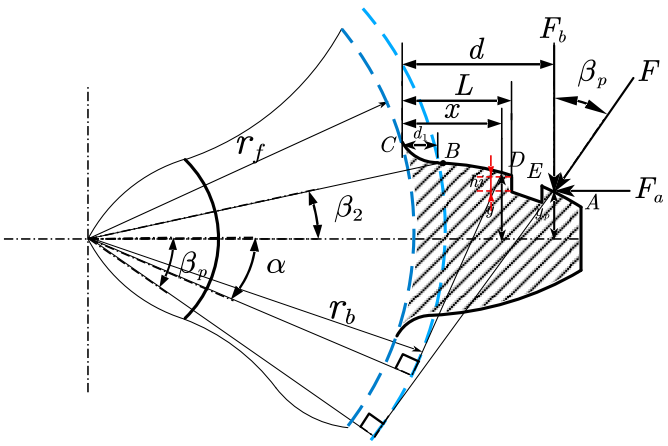

Figure 2. Sketch map of a spall spur gear tooth.

The gear with spalling failure can be viewed as a non-uniform cantilever beam, as shown in the figure.2, D, E two points are the beginning and end of spalling meshing point, according to the location of spalling will be divided into three segments of the meshing interval, which can be obtained from the pinion compression, bending and shear energy:

IF $x_B \le x_p < x_D$:

$$\begin{aligned} U_a &= \int_{x_C}^{x_B} \frac{F_a^2}{2EA_{1x}} dx_1 + \int_{x_B}^{x_P} \frac{F_a^2}{2EA_{2x}} dx_2 \\ U_a &= \int_{x_C}^{x_B} \frac{F_a^2}{2EA_{1x}} dx_1 + \int_{x_B}^{x_P} \frac{F_a^2}{2EA_{2x}} dx_2 \\ U_s &= \int_{x_C}^{x_B} \frac{1.2F_b^2}{2GA_{1x}} dx_1 + \int_{x_B}^{x_P} \frac{1.2F_b^2}{2GA_{2x}} dx_2 \end{aligned} \tag{2}$$

ELSE IF $x_D \le x_p < x_E$:

$$\begin{aligned} U_a &= \int_{x_C}^{x_B} \frac{F_a^2}{2EA_{1x}} dx_1 + \int_{x_B}^{x_D} \frac{F_a^2}{2EA_{2x}} dx_2 + \int_{x_D}^{x_P} \frac{F_a^2}{2EA_s} dx_2 \\ U_b &= \int_{x_C}^{x_B} \frac{M_{1x}^2}{2EI_{1x}} dx_1 + \int_{x_B}^{x_D} \frac{M_{2x}^2}{2EI_{2x}} dx_2 + \int_{x_D}^{x_P} \frac{M_{2x}^2}{2EI_s} dx_2 \\ U_s &= \int_{x_C}^{x_B} \frac{1.2F_b^2}{2GA_{1x}} dx_1 + \int_{x_B}^{x_D} \frac{1.2F_b^2}{2GA_{2x}} dx_2 + \int_{x_D}^{x_P} \frac{1.2F_b^2}{2GA_s} dx_2 \end{aligned} \tag{3}$$

ELSE $x_E \le x_p$:

$$\begin{aligned} U_a &= \int_{x_C}^{x_B} \frac{F_a^2}{2EA_{1x}} dx_1 + \int_{x_B}^{x_D} \frac{F_a^2}{2EA_{2x}} dx_2 + \int_{x_D}^{x_E} \frac{F_a^2}{2EA_s} dx_2 + \int_{x_{x_E}}^{x_P} \frac{F_a^2}{2EA_{2x}} dx_2 \\ U_b &= \int_{x_C}^{x_B} \frac{M_{1x}^2}{2EI_{1x}} dx_1 + \int_{x_B}^{x_D} \frac{M_{2x}^2}{2EI_{2x}} dx_2 + \int_{x_D}^{x_E} \frac{M_{2x}^2}{2EI_s} dx_2 + \int_{x_E}^{x_P} \frac{M_{2x}^2}{2EI_{2x}} dx_2 \\ U_s &= \int_{x_C}^{x_B} \frac{1.2F_b^2}{2GA_{1x}} dx_1 + \int_{x_B}^{x_D} \frac{1.2F_b^2}{2GA_{2x}} dx_2 + \int_{x_D}^{x_E} \frac{1.2F_b^2}{2GA_s} dx_2 + \int_{x_E}^{x_P} \frac{1.2F_b^2}{2GA_{2x}} dx_2 \end{aligned} \tag{4}$$

Where E is the modulus of elasticity, G is the shear modulus. $F_a = Fsin\beta_p$, $F_b = Fcos\beta_p, M_a = Fsin\beta_p \times y_p. F_a, F_b$ are the numerical and horizontal components of the meshing force of the gear teeth, respectively. β_p is the angle between the meshing line and the y-axis at any position p. x_1, x_2 are the horizontal coordinates of the transition curve and the asymptote, respectively. $x_C, x_B, x_{D,} x_E, x_A$ are the starting point of transition curve C, starting point of involute B, starting point of flaking D, termination point of flaking E, and termination point of involute A. $A_{ix} = 2y_i w;\ M_x = F_b(x_p - x) - F_a y_p;\ I_{ix} = \frac{2}{3} y_i^3 w$; are the cross-sectional area of the gear tooth, bending moment and cross-sectional inertia of the gear tooth at the point of mesh away from the tooth root x, and the bending moment and cross-sectional inertia of the wheel tooth at the point of mesh away from the tooth root. i=1,2,s are the transition curve, the normal section of the involute and the cross-section of the spalling region.

The interface contact line length ls, cross-sectional area As and cross-sectional moment of inertia Is at the spalling area:

$l_s = W - w_i, A_S = 2y_x W - y_i w_i,$

$$I_S = \frac{2}{3} y_x^3 W - \frac{1}{3} w_i (y_x^3 - (y_x - h_i)^3) \tag{5}$$

The Hertzian contact stiffness at the time of spalling emergence is obtained from the change in Hertzian contact stiffness in the normal meshing region and the length of the meshing contact line:

$$k_{h=} \begin{cases} \dfrac{E^{0.9} W^{0.8} Fm^{0.1}}{1.275} & healthy \\ \dfrac{E^{0.9} (W - wi)^{0.8} Fm^{0.1}}{1.275} & spalled \end{cases} \tag{6}$$

The base elastic stiffness of the gear is calculated as follows:

$$\frac{1}{k_f} = \frac{\cos^2 \alpha}{EW} \left[L^*(h, \theta_f) \left(\frac{u}{S_f} \right)^2 + M^*(h, \theta_f) \frac{u}{S_f} + P^*(h, \theta_f) \left[1 + Q^*(h, \theta_f) \tan^2 \alpha \right] \right] \tag{7}$$

The combined meshing stiffness of the gear pair is:

$$k_m = \begin{cases} \dfrac{1}{\frac{1}{k_h} + \frac{1}{k_{ap}} + \frac{1}{k_{bp}} + \frac{1}{k_{sp}} + \frac{1}{k_{fp}} + \frac{1}{k_{ag}} + \frac{1}{k_{bg}} + \frac{1}{k_{sg}} + \frac{1}{k_{fg}}} & \text{sin}\, gle \quad tooth \\ \sum_{i=1}^{2} \dfrac{1}{\frac{1}{k_{hi}} + \frac{1}{k_{api}} + \frac{1}{k_{bpi}} + \frac{1}{k_{spi}} + \frac{1}{k_{fpi}} + \frac{1}{k_{agi}} + \frac{1}{k_{bgi}} + \frac{1}{k_{sgi}} + \frac{1}{k_{fgi}}} & double \quad tooth \end{cases} \tag{8}$$

Where i=1,2 are the first pair of gear pair and the second pair of gear pair during meshing respectively.

2.2. Time-varying Meshing Stiffness Model for Asymmetrically Distributed Spalling based on the Slicing Method

The physical model of an asymmetrically distributed spalled tooth pair based on the slicing method is shown in Fig. 3(b) shows the load distribution at the meshing line A-A in Fig.3(a). The red dashed line indicates the homogeneous load at the normal cross-section, and the blue dashed line indicates

that the load is no longer homogeneous at the meshing line B-B (which is on the right side of the meshing line A-A) caused by spalling.

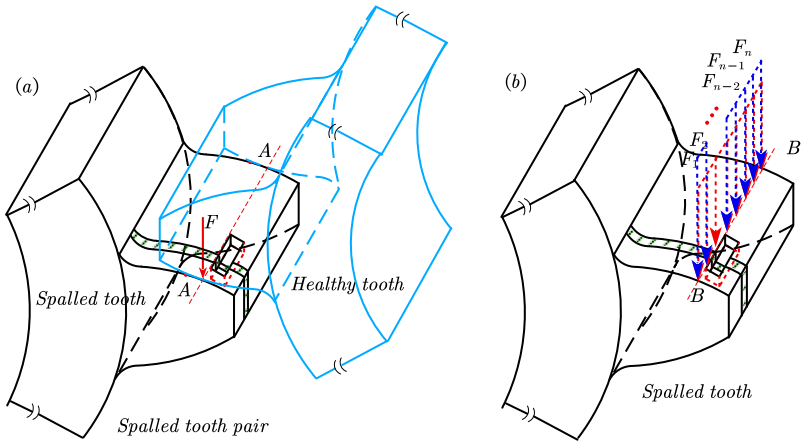

Figure 3. Sketch of asymmetrically distributed spalled spur gear teeth.a),b)

In order to establish the coupling relationship between the tooth blade stiffness and the load distribution along the TWD direction, a parallel stiffness model of the asymmetrically spalled tooth blade was developed, as shown in Fig. 4, which is mainly divided into two types: spalled and healthy. Unlike the teeth in the healthy tooth pair, the load F_sj along the TWD direction of the asymmetrically spalled teeth leads to additional torsional deformation. Therefore, in order to represent the torsional deformation of each piece under the load F_sj, the torsional stiffness is added to the stiffness of the tooth piece proposed with asymmetric flaking, as represented by k_{stj}or k_{htj} in Fig. 4. In addition, due to the uniform distribution of stiffness and load along the TWD direction, the deformations of the tooth slices along the TWD direction are not equal, which will result in coupling forces between neighboring tooth slices. And the conventional models usually ignore the piece coupling effect [13,14,23-26]. Therefore, in the parallel slice stiffness model proposed in this paper, the slice coupling stiffness is also added to model the coupling effect between the slices, which is represented by the red spring$k_{sp(j-1)j}$in Fig. 4.

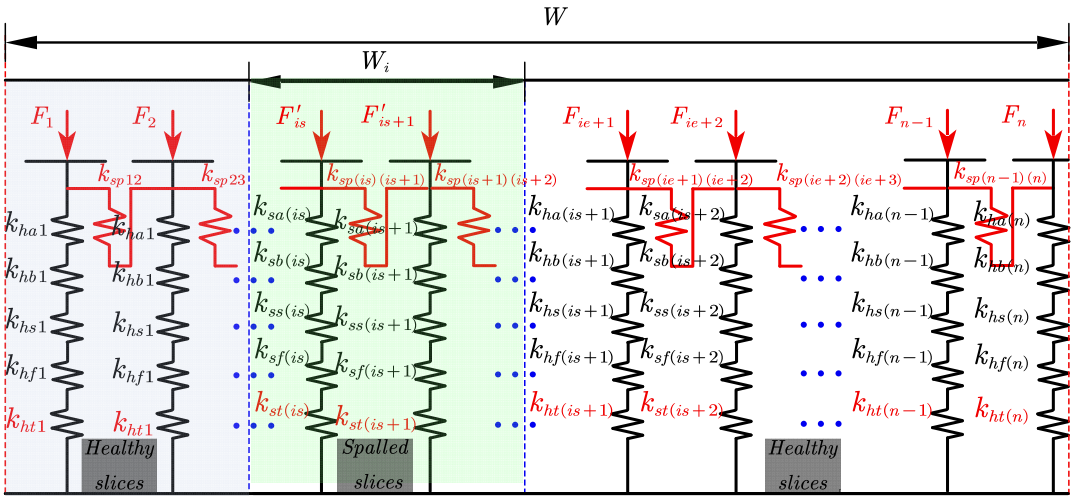

Figure 4. Parallel slice stiffness model of the tooth with ESC.

2.3. Analytical Modeling of Tooth Torsional Deformation

The tooth torsional stiffness of each piece along the TWD direction is the primary prerequisite for establishing the analytical TVMS expression for the proposed parallel piece stiffness model. Since the existing tooth torsional deformation calculation formulas in the literature are unable to obtain the

torsional force arm of the tooth at a specific position along the TWD, the actual torsional deformation cannot be obtained, and they cannot be directly used in the proposed parallel-slice stiffness model, a new analytical model of tooth torsional deformation is established in this section.

The physical model for calculating the torsional deformation of the tooth blade using asymmetric flaking is shown in Fig. 5. As shown in Fig. 5 (a), due to the presence of flaking, the deformation regions of flaked teeth are as follows I region is the normal deformation region during the meshing process of the wheel teeth, II region is the torsion region affected by flaking, and III region is affected by the II region which will produce a slight torsion. Where A-A is the cross-section at the meshing point. $F_c$is the meshing force of the spalled tooth, and F_a and F_b are the radial compression force and axial shear force decomposed by the meshing force Fc. Fig. 5 (b) shows a schematic diagram of the torsional deformation of cross section A-A. In Fig. 5(b), the rectangle ABCD represents the actual cross-section A-A of the spalled tooth, and the folded line EFGH represents the spalled pit. Points O_0 and O_2 denote the centers of mass of the rectangle ABCD and the fold line EFGH of the pit, respectively. The coordinate system $Y_0O_0Z_0$ refers to the right-angle coordinate system established with O_0 as the origin. Therefore, the actual shape of the deformed region of section A-A is AEFGHBCD, and its center of mass is O_s. The deviation distances of $O_s$from the 的$Y_0$and Z_0 axes of the original coordinate system $Y_0O_0Z_0$ are ΔZ and ΔY, respectively. The shaded part denotes the jth slice, whose width is ΔW. $\rho_{(j)}$ denotes the position of the jth slice in the coordinate system in terms of the coordinates of the Z_0 axis, i.e., the jth slice's spalling torsion force arm. A row of arrows indicates the uneven load along the tooth width direction of the flaked tooth subassembly, where the red arrow indicates the shear force F_{bj} acting on the jth slice. $\delta_{tsj}$is the torsional deformation of the tooth j_{th}slice.

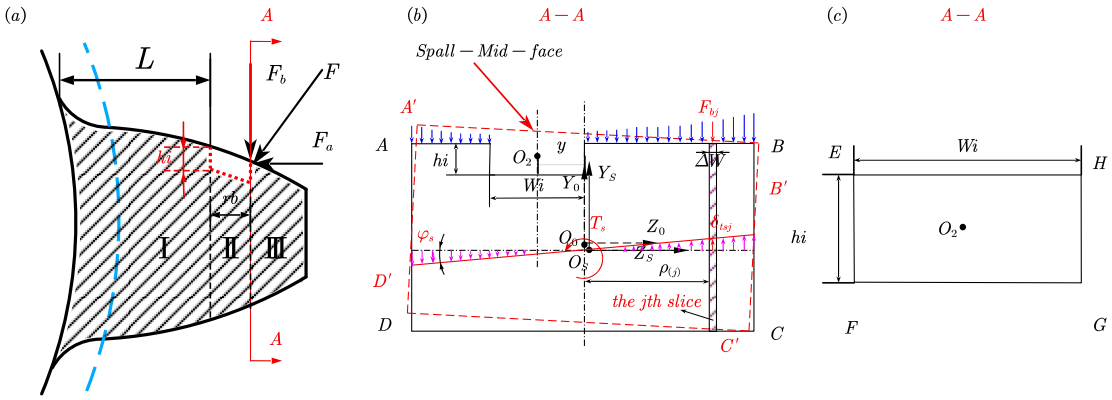

Figure 5. Parallel slice stiffness model of the tooth with spalled.

Gears with asymmetrically distributed spalling are categorized into three cases depending on the location of the defect offset, as shown in the figure.

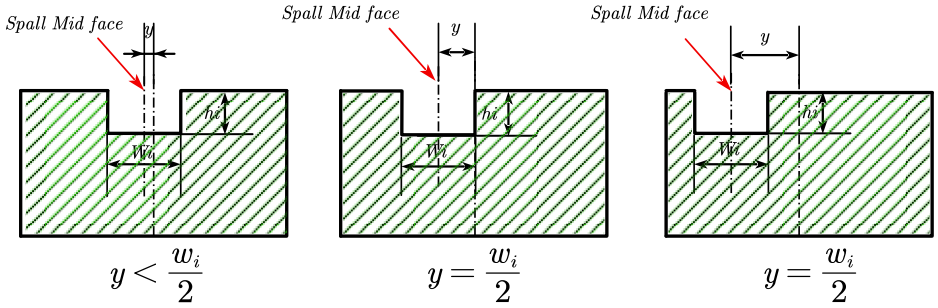

Figure 6. Shape change of the cross-sections due to spalling.

Different spalling locations correspond to different torsional force arm lengths, for which equivalent arm functions are listed:

$$\rho_{(j)}=\begin{cases}\dfrac{2y}{n}j+(\dfrac{w_i}{2}-y) & y<\dfrac{w_i}{2}\\ \dfrac{w_i}{n}i & y=\dfrac{w_i}{2}\\ \dfrac{w_i}{n}j+(y-\dfrac{w_i}{2}) & \dfrac{w_i}{2}<y\le\dfrac{w-w_i}{2}\end{cases} \tag{9}$$

Where $\rho_{(j)}$ represents the torsional force arm length of the jth piece, j=1, 2, ..., n. y is the distance between the center of the spalling position and the centerline of the tooth width, and w_i is the spalling length.

The torque generated by the gear tooth in the interval of the spalling position:

$$T_s=\sum_{j=1}^{n_s}F_{bj}\rho_{(j)} \tag{10}$$

where F_{bj}denotes the shear force acting on the jth slice, n: the number of slices in the tooth width direction, n_s: the number of slices occupied by the area affected by spalling.

According to the energy method, the gear tooth bending torsional energy is obtained:

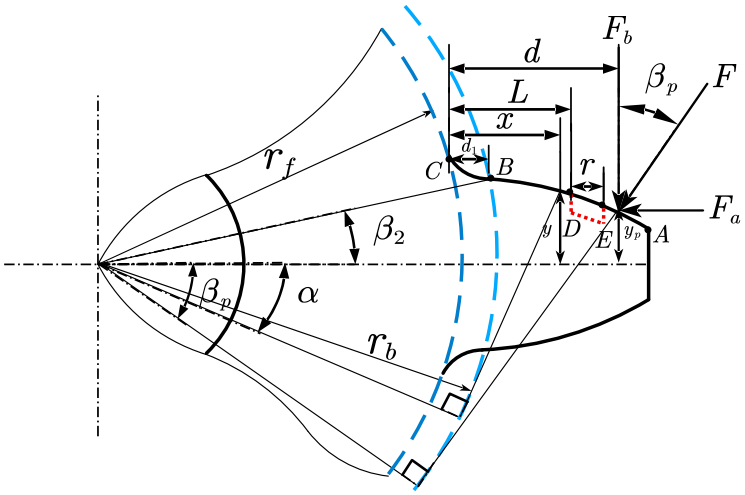

Figure 7. cantilever beam model of asymmetrically distributed spalled.

$$V_\varepsilon=W=\frac{1}{2}T_s\varphi_s=\frac{T_s^2l}{2GI_P} \tag{11}$$

$$U_t=\frac{F_b^2}{2k_t}=\int_{x_c+L}^{x_c+L+r}\frac{T_s^2}{2GI_P}dx_2 \tag{12}$$

Where, x_c+L is the starting position of the spalling interval on the involute transverse coordinate, andx_c+L+r is the termination position of the spalling interval. T_s is the spalling torque, φ_s is

the torsion angle , l is the length of the gear tooth in the spalling affected interval, G is the shear modulus, and I_p is the polar moment of inertia of the spalled section .

To facilitate the calculation, the coordinates of the flaking start position are converted to the meshing angle β_s,β_e. According to the torsional bending deformation energy to obtain the pinion torsional stiffness formula:

$$\frac{1}{k_{tp}} = \int_{\beta_s}^{\beta_e} \frac{\left(\sum_{i=1}^{n} \rho_{(i)}\right)^2}{GI_{Pp}} r_b(\beta_2 + \beta)\cos\beta d\beta \tag{13}$$

Where, k_tp is the pinion torsional stiffness and β_2 is the base circle half angle of the pinion involute tooth profile.

3. MODEL VERIFICATION AND DISCUSSION

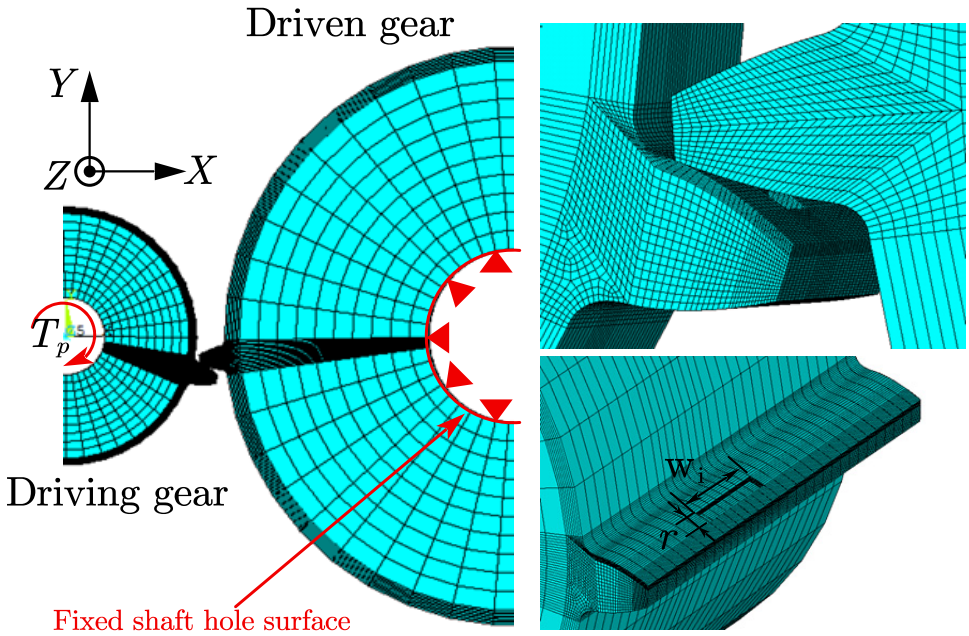

Figure 8. FE model for calculating the TVMS.

In order to verify the correctness and accuracy of the proposed asymmetric spalling model and to consider the effect of asymmetric spalling, a finite element model for calculating the TVMS of asymmetric distributed spalled gears is established by using the Solid185 unit, and in order to improve the efficiency of the calculation and to simplify the three-dimensional model, only one pair of teeth is established, assuming that the other normal teeth have no effect on the mesh stiffness, and the main attention is paid to the effect of spalling. Define the contact unit Conta174 and the target unit Targe170 to establish a single pair of wheel teeth contact model, as shown in Fig.8 The finite element model boundary conditions are set as follows:Fix the driven wheel shaft bore and constrain its degrees of freedom. The active wheel is constrained to have degrees of freedom other than those that allow it to rotate along the z-axis. A torque T_p, is applied to the aperture of the active wheel in the z-axis direction, and the torsional angular deformation $\Delta\theta_f$ is extracted on the aperture of the active wheel in the direction of the z-axis rotation.Under the action of the torque T_p, the finite element model calculates the TVMS equation as follows [28]:

$$K_{t(FE)} = \frac{T_P}{\Delta\theta_f R_b^2} \tag{14}$$

The following figure.8 shows the theoretical calculations and finite element results:

In this section, the effects of the spalling length on TVMS are investigated. Under different spalling widths TVMS at ws = 0 mm ,16 and 30 mm Difference in time-varying meshing stiffness for spallation models with and without torsion are shown in Fig.11, Fig.12 ,Fig.9 and Fig .10.respectively.These figures show the following phenomena:

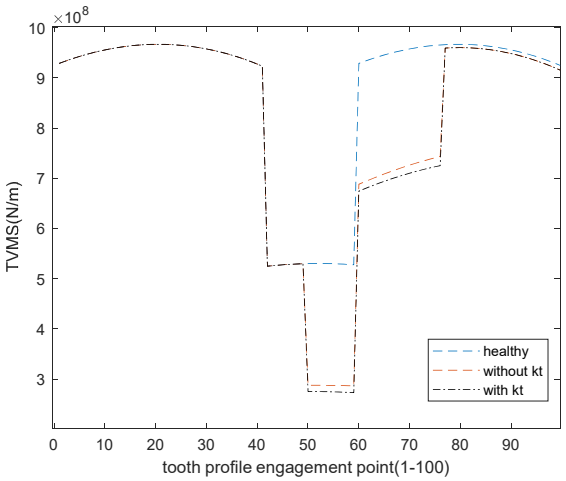

Figure 9. TVMS with or without torsion

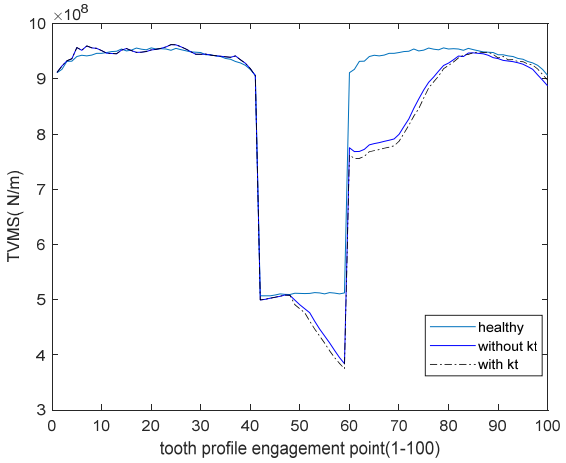

Figure 10. Finite element validation results

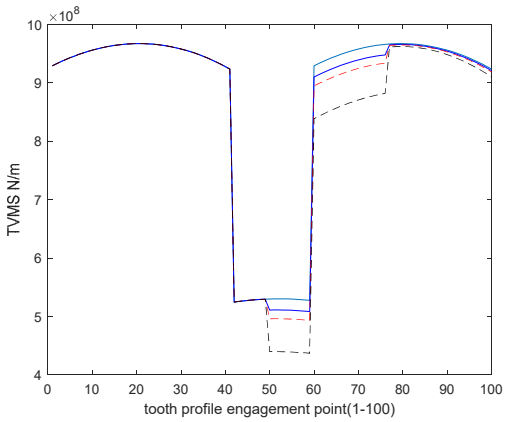

Figure 11. Effect of flaking length on TVMS

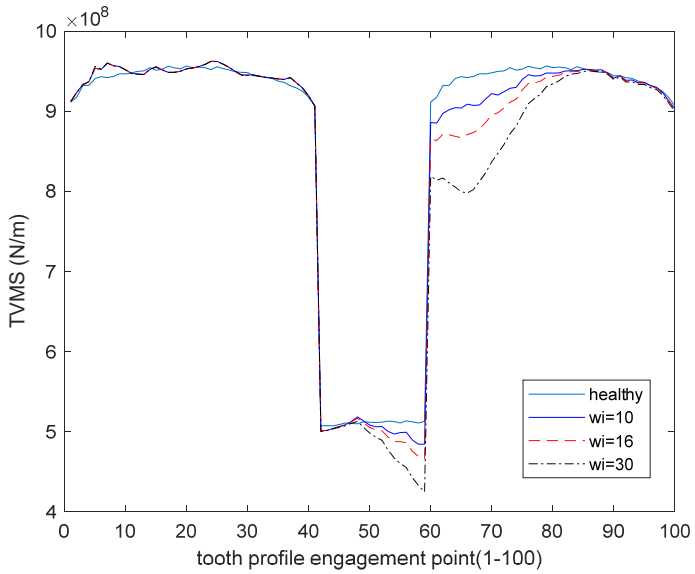

Figure 12. Finite element validation results

4. CONCLUSION

In this paper, the effect of time-varying meshing stiffness of a tooth spalling gear pair with torsion is considered. An improved analytical method is established based on the vertical cut method of the gear teeth. By comparing the TVMS with the TVMS derived from the finite element (FE) method was validated. Some of the conclusions are summarized below:

(1) When the spalling width is small, the TVMS obtained by the proposed method agrees very well with that obtained by the FE method;

(2) When the spalling width is smaller. However, there are still some large errors at larger spalling widths because larger spalling widths result in a smaller contact area, which leads to uneven load distribution and consequently gear deformation.

A large spalling width leads to uneven load distribution, which in turn leads to the gear deformation obtained from the FE method.

of the gear deformation will be larger than the method proposed in this paper. In addition, in terms of computational efficiency, the proposed method is superior to the FE method.

(3) As the spalling width increases, the TVMS decreases dramatically, especially in the single-tooth engagement region. In addition, asymmetric flaking makes the wheel tooth stiffness increase due to the generation of torsional stiffness, which produces a decrease in TVMS.

CONFLICTS OF INTEREST

The authors declare that they have no conflict of interest.

ACKNOWLEDGMENTS

The authors thank the National Natural Science Foundation of China (Grant No. 52375104).

REFERENCES

[1] A. Haris, E. Motato, S. Theodossiades, et al., A study on torsional vibration attenuation in automotive drivetrains using absorbers with smooth and non-smooth nonlinearities, Appl. Math. Model, 46 ,674–690, 2017.

[2] B. Mashadi, M. Badrykoohi, Driveline oscillation control by using a dry clutch system, Appl. Math. Model,39 (21) 6471–6490, 2015.

[3] Li, S., Kahraman, A.: Influence of dynamic behaviour on elastohydrodynamic lubrication of spur gears. Inst. Mech.Eng. 225(8), 740–753 ,2011.

[4] Pizzolante, F., Battarra, M., D'Elia, G., et al.: A rattle index formulation for single and multiple branch geartrains.Mech. Mach. Theory 158, 104246 ,2021.

[5] Meng, Z., Shi, G., Wang, F.: Vibration response and fault characteristics analysis of gear based on time-varying mesh stiffness. Mech. Mach. Theory 148, 103786 ,2020.

[6] Liu, F., Jiang, H., Liu, S., et al.: Dynamic behavior analysis of spur gears with constant & variable excitations considering sliding friction influence. J. Mech. Sci. Technol.30(12), 5363–5370 ,2016.

[7] L. Wang, Y. Shao, Fault mode analysis and detection for gear tooth crack during its propagating process based on dynamic simulation method, Eng. Fail. Anal. 71,166–178, 2017.

[8] F. Chaari, T. Fakhfakh, M. Haddar, Analytical modelling of spur gear tooth crack and influence on gearmesh stiffness, Europ. J. Mech. - A/Solids 28 , 461–468,2009.

[9] D.C.H. Yang, J.Y. Lin, Hertzian damping, tooth friction and bending elasticity in gear impact dynamics, J. Mech. Transm. Autom. Des. 109 ,189–196,1987.

[10] X.H. Tian, Dynamic Simulation for System Response of Gearbox Including Localized Gear FaultsM.S. thesis University of Alberta, Edmonton, 2004.

[11] S. Wu, Gearbox Dynamic Simulation and Estimation of Fault GrowthM.S. thesis University of Alberta, Edmonton, 2007.

[12] S. Jia, I. Howard, Comparison of localised spalling and crack damage from dynamic modelling of spur gear vibrations, Mech. Syst. Signal Process. 20 , 332–349,2006.

[13] Yang L, Wang L, Shao Y et al A double-layer iterative analytical model for mesh stiffness and load distribution of early-stage cracked gear based on the slicing method[J]. Mech Syst Signal Process 198:110456,2023.

[14] Z. Meng, G. Shi, F. Wang, Vibration response and fault characteristics analysis of gear based on time-varying mesh stiffness, Mech. Mach. Theory 148 103786,2020.

[15] L. Yang, Y. Shao, W. Jiang, L. Zhang, L. Wang, J. Xu, Effects of tooth surface crack propagation on meshing stiffness and vibration characteristic of spur gear system, Appl. Sci. 11 (4) 1968,2021.

[16] F. Chaari, W. Baccar, M.S. Abbes, M. Haddar, Effect of spalling or tooth breakage on gearmesh stiffness and dynamic response of a one-stage spur gear transmission, Eur. J. Mech-A/Solid,27 691–705, 2008.

[17] Y.M. Shao, X.L. Wang, J. Liu, Z.G. Chen, Time-varying stiffness model and dynamic response characteristics of gears with tooth surface spalling and edge contact, J. Vib. Shock.,33 8–14, 2014.

[18] R. Ma, Y.S. Chen, Q.J. Cao, Research on dynamics and fault mechanism of spur gear pair with spalling defect, J. Sound Vib, 331 2097–2109,2012.

[19] R. Ma, Y.S. Chen, Research on the dynamic mechanism of the gear system with local crack and spalling failure, Eng. Fail. Anal.,26,12–20,2012.

[20] H.J. Jiang, Y.M. Shao, C.K. Mechefske, Dynamic characteristics of helical gears under sliding friction with spalling defect, Eng. Fail. Anal.,39 92–107,2014.

[21] A. Saxena, A. Parey, M. Chouksey, Time varying mesh stiffness calculation of spur gear pair considering sliding friction and spalling defects, Engineering Failure Analysis 70200–211,2016.

[22] Saxena A, Parey A and Chouksey M. Effect of shaft misalignment and friction force on time varying mesh stiffness of spur gear pair. Eng Fail Anal,49: 79–91,2015.

[23] L. Han, H. Qi, Influences of tooth spalling or local breakage on time–varying mesh stiffness of helical gears, Eng. Fail. Anal, 79 ,75–88,2017.

[24] Wang F, Dai P, Yan S, et al. Investigation on double shock in vibration response of the gear pair with spalling defects[J]. Proceedings of the Institution of Mechanical Engineers, Part C: Journal of Mechanical Engineering Science, 237(20): 4882-4894,2023.

[25] Xue, S., Howard, I., Wang, C., et al.: Dynamic modelling of the gear system under non-stationary conditions using the iterative convergence of the tooth mesh stiffness. Eng. Fail. Anal,131, 105908,2022.

[26] Guan, X., Tang, J., Hu, Z., et al.: A new dynamic model of light-weight spur gear transmission system considering the elasticity of the shaft and gear body. Mech. Mach. Theory 170, 104689, 2022.

[27] Ma R, Chen Y. Bifurcation of multi-freedom gear system with spalling defect[J]. Applied Mathematics and Mechanics, 34: 475-488,2013.

[28] Luo Y, Baddour N, Liang M. A shape-independent approach to modelling gear tooth spalls for time varying mesh stiffness evaluation of a spur gear pair[J]. Mechanical Systems and Signal Processing ,120: 836-852,2019.